Universal Law for Diffusion in Continuous Potential Energy Landscapes

Bohan Yu,[1,2] Luhui Ning,[1,2,3] and Ke Chen[1,2,4,*]

[1]Beijing National Laboratory for Condensed Matter Physics and Laboratory of Soft Matter Physics, Institute of Physics, Chinese Academy of Sciences, Beijing 100190, People's Republic of China

[2]School of Physical Sciences, University of Chinese Academy of Science, Beijing 100049, People's Republic of China

[3]Beijing Key Laboratory of Optical Detection Technology for Oil and Gas, China University of Petroleum–Beijing, Beijing 102249, People's Republic of China

[4]Songshan Lake Materials Laboratory, Dongguan, Guangdong 523808, China

(Received 21 February 2025; accepted 17 November 2025; published 4 December 2025)

Using video microscopy and computer simulations, we study the diffusion dynamics of colloidal particles in continuous potential energy landscapes at quasi-two-dimensions. The potential energy landscapes are constructed using scanning optical tweezers in the experiments, and the diffusion coefficients are extracted from the long-time mean squared displacements of tracer particles. We discover a universal relation that quantitatively determines the normalized long-time diffusion coefficient of a colloidal particle from the shape of the potential energy landscape, characterized by the Shannon information entropy S_N and a generalized packing fraction ϕ. This relation is validated in a wide range of potential distributions, and over a large dynamic range. As all elemental diffusions can be considered as a dynamical process of exploring an external potential energy landscape by a diffusing particle, this universal law, which reduces multidimensional potential distributions to two dimensionless numbers, provides a quantitative tool to study dynamical phenomena in a wide range of complex environments, where general analytical or empirical models are lacking.

DOI: 10.1103/39zl-5pn3

Diffusion is a fundamental process that determines the dynamics of many physical systems. The simplest diffusion is the Brownian motion of a colloidal particle in homogeneous Newtonian fluid, which can be quantitatively described by the Langevin equation. In practice, however, diffusion often occurs in systems with complex structures and interactions. Examples include electron diffusions in composite materials [1–3], macromolecules in polymeric or biological systems [4–7], colloids in visco-elastic fluids [8–10], transport of nanoparticles in porous media [11–13], and the unusual dynamics during glass transitions [14–16]. In these systems, particles diffuse in a spatially and/or temporally heterogeneous potential energy landscape (PEL). The diffusion rates are sensitive to small changes of system parameters such as composition, structure, density, or temperature.

Theoretical analysis of diffusion in nontrivial PELs is challenging, with quantitative predictions available only for a few special cases. Existing theories can be divided into two categories. The first category models the diffusion process as hoppings between discrete sites, including the continuous time random walk model [17], the random barrier model [18], the random trap model [19,20], and diffusion in periodic or rough potentials [21–25]. When the distance between two adjacent sites is λ, the diffusion coefficient is given by $D = \Gamma_{\text{eff}}\lambda^2/2d$, where Γ_{eff} is the effective transition rate to be obtained and d is the dimension of the system. The second category focuses on many-particle systems. Earlier work by Rosenfeld [26,27] and Dzugutov [28] connect the dimensionless diffusion coefficient to the excess entropy in dense fluids by

$$D^* = Ce^{AS_{\text{ex}}}. \tag{1}$$

The excess entropy arises from the intercorrelations between diffusing particles, and is defined as the difference between the thermal entropy of the system S_{sys} and the entropy of an ideal gas under equivalent conditions S_{id}, with $S_{\text{ex}} = S_{\text{sys}} - S_{\text{id}}$. This simple relation is later revised using kinetic collision theories by Samanta *et al.* [29–31] and Ning *et al.* [32] to correct for density effect and solvent viscosity, and is verified in colloidal experiments for a wide range of densities. A recent theoretical study by Sorkin *et al.* [33] derives a rigorous inequality which prescribes a general bound for diffusion coefficient as a function of entropy. However, neither of the two groups of theories can be extended to the scenarios of the other, or to the general situation of a particle diffusing in a smooth continuous potential energy landscape at two or three dimensions.

In this Letter, we investigate the diffusing dynamics of colloidal particles in a wide range of continuous PELs, constructed by optical tweezers and frozen colloidal

*Contact author: kechen@iphy.ac.cn

particles using video microscopy experiments. We obtain a universal relation that uniquely determines the long-time diffusion coefficient from the shape of the PEL. The experimental results are further tested and validated by computer simulations over a large variety of PELs. Two relevant parameters are identified: one is the normalized information entropy S_N of the PEL, and the other is the generalized packing fraction ϕ which measures the spatial fluctuations of the PEL. This general relation establishes a critical link between thermodynamics and dynamics in complex systems, and provides a powerful tool for structure-dynamics problems in condensed matter physics.

The samples consist of dilute suspensions of polystyrene (PS) tracer spheres (1 μm in diameter) confined between two coverslips, forming a quasi-2D system in which the particles can diffuse freely. The PELs are constructed by scanning laser tweezers (Aresis Tweez 250si, wavelength 1064 nm) in the field of view. Focused laser beam creates an attractive potential to colloidal particles with a range of ~2 μm. The shape of the potential field of an optical trap can be approximated by a Gaussian function. By scanning the traps over the field of view, and adjusting the intensity and repetition frequency of the optical traps at each point, a continuous PEL is constructed. Several patterns of the PELs are used in our experiments, including discrete arrays of Gaussian traps, both crystalline or disordered; discrete arrays of non-Gaussian traps or double wells, created by overlapping two optical traps of different intensity; and smooth random potentials realized by scanning defocused laser beams. In addition, purely repulsive backgrounds are formed by frozen colloidal particles. The intensity of the optical traps or the density of the frozen background is controlled so that the diffusing particles can frequently escape from local constraints on the timescale of the experiment. The lattice constant for square or triangular lattices of optical traps varies from 5.0 to 12.0 μm, and the number density for disordered lattices ranges from 0.009 to 0.026 μm^2.

The shape of the PELs are determined from the measured probability density distribution of the tracers using the Boltzmann relation with $P(\mathbf{r}) = e^{-U(\mathbf{r})/k_BT} / \sum e^{-U(\mathbf{r})/k_BT}$. All the PELs in our experiments satisfy the unbiased condition which is tested by fitting the PELs to a 2D plane. Figure 1(a) shows a snapshot of the experiment where red crosses indicate the locations of optical traps in a square lattice. The measured PEL is shown in Fig. 1(b), and is fit to a 2D plane with negligible biases. Additional PELs from the experiments can be found in Supplemental Material [34]. The trajectories of the tracer particles are recorded by digital video microscopy, and extracted using particle tracking software. The long-time diffusion coefficients of colloidal particles are measured by linearly fitting the mean squared displacements of the particles at long times using $\langle \Delta\mathbf{r}^2(t) \rangle = 4Dt$.

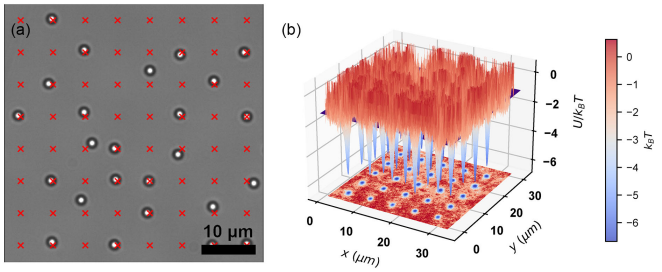

FIG. 1. Colloidal particles diffusing in a PEL formed by optical tweezers. (a) A snapshot of the experiments. PS particles (bright spots) diffuse in a square lattice of optical tweezers (red crosses) (b) Measured potential energy landscape in (a). The PEL is fitted to a plane (purple) with $U(x, y) = -1.20 - 1.07 \times 10^{-3}x + 4.30 \times 10^{-4}y$.

In addition to colloidal experiments, we also perform Brownian dynamics simulations to a wider range of PELs at 2D. In the simulations, optical traps are modeled by Gaussian potential wells, and fixed background particles are simulated by repulsive Lennard-Jones (LJ) barriers. Besides the configurations of traps and barriers in the experiments, the simulations employ PELs constructed from cosine-squared potentials and adjusted Gaussian random potentials as examples for random smooth potentials that are more general than patterns of point potentials (Supplemental Material [34]).

To establish a quantitative relation between diffusing dynamics and the PEL, we first consider two extreme situations. The first one is the case of a single negative delta potential $-\delta(\mathbf{r} - \mathbf{r}_0)$ where the particle is permanently trapped at position $\mathbf{r}_0$ with a diffusion coefficient $D \to 0$ (Supplemental Material [34]). The second situation is a completely flat PEL, where the expected diffusion coefficient is D_0, as predicted by the Stokes-Einstein relation. These two PELs can be parametrized by the information entropy from the spatial distribution of potential energy, using Boltzmann relation and the Shannon entropy formula, with $S = -\sum_i P_i \ln P_i$, where P_i is the probability of finding a diffusing particle at $\mathbf{r}_i$. At equilibrium, $P_i \propto \exp[-U(\mathbf{r}_i)/k_BT]$, where k_B is the Boltzmann constant, and T is the absolute temperature. The flat PEL and the negative delta trap correspond to the maximum ($S_{\max}$) and minimum information entropy ($S \to 0$) for PELs in a given space respectively, which coincide with the maximum and minimum of diffusion coefficients in equilibrium. Inspired by the classical Adam-Gibbs scaling relation [37], we propose a simple relation between the diffusion coefficient and the information entropy of the PELs that satisfies these two extreme conditions

$$\ln \frac{D}{D_0} = -\alpha \left(\frac{S_{\max}}{S} - 1 \right), \qquad (S \neq 0), \tag{2}$$

where α is a dimensionless factor. By defining a normalized entropy $S_N = S/S_{\max}$, we arrive at

$$\ln\frac{D}{D_0} = -\alpha\left(\frac{1}{S_N} - 1\right), \qquad (S_N \neq 0). \tag{3}$$

In practice, the information entropy S can be obtained by dividing the field of view into N bins, and measuring the probability of finding a particle in the ith bin, P_i, after the PEL is adequately explored (Supplemental Material [34]). The maximum entropy under the same partition is $S_{\max} = \ln N$, which corresponds to the uniform distribution on a flat PEL.

Figure 2 plots $\ln(D/D_0)$ as a function of $(1/S_N - 1)$ for colloidal particles diffusing in crystalline lattices of optical traps. Given the pattern of a lattice (symmetry and lattice constant), the diffusing dynamics is tuned by varying the intensity of individual traps. The measured diffusion coefficient and information entropy indeed follow Eq. (3). The fitted slope α, however, is not a constant across different patterns, which suggests that S_N is not the sole factor that determines diffusing dynamics in PELs. The apparent difference between the crystalline patterns in Fig. 2 is the number density of the traps, with steeper slopes for patterns with higher trap densities. To account for the trap density, we introduce a generalized packing fraction ϕ defined as $\phi = 1 - \langle \exp[-(\Delta U/2k_BT)^2]\rangle$, where $\Delta U = U - \bar{U}$ is the difference between local potential energy

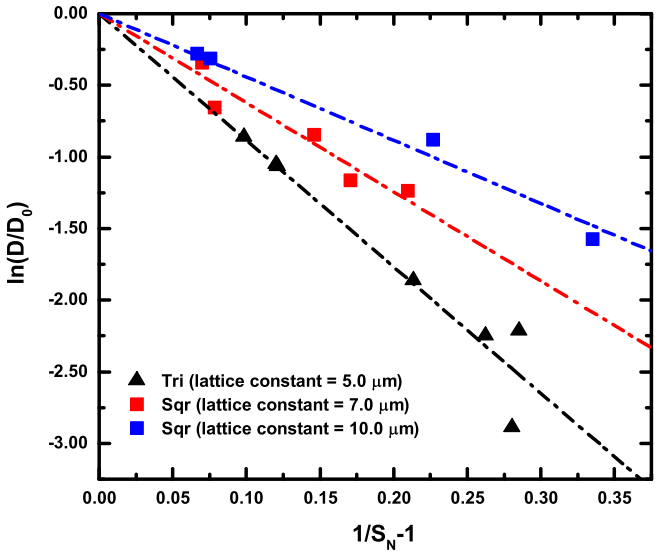

FIG. 2. The normalized long-time diffusion coefficient as a function of normalized information entropy. Different symbols represent results from different crystalline lattices of optical traps, including square lattice with a lattice constant of 10.0 μm (blue squares), square lattice with a lattice constant of 7.0 μm (red squares) and triangular lattice with a lattice constant of 5.0 μm (black triangles). The dash-dotted lines are linear fits of the corresponding data of the same colors by Eq. (3).

$U(r)$ and the fitted flat plane $\bar{U}(r)$, and $\langle\cdot\rangle$ is an average over all locations. ϕ characterizes regions where local potential energy significantly deviates from the unbiased baseline, including both barriers and wells. When applied to systems consisting of solid particles barriers, ϕ recovers the conventional packing fraction. Like S_N, ϕ is only a function of the PEL, and can be easily extended to continuous PELs where regions may not be clearly identified as discrete traps or barriers.

The experimental results can now be collapsed by a modified equation,

$$\ln\frac{D}{D_0} = -\alpha_0\phi^{0.5}\left(\frac{1}{S_N} - 1\right), \qquad (S_N \neq 0), \tag{4}$$

where α_0 is the new dimensionless fitting parameter. Figure 3(a) shows the normalized diffusion coefficient as a function of $\phi^{0.5}[(1/S_N) - 1]$ for backgrounds constructed by optical tweezers (solid symbols) and the fitted line to Eq. (4) (dashed line). For comparison, results from backgrounds of fixed colloidal particles are also shown in Fig. 3(b) (stars). In the experiments, the diffusion coefficient changes by a factor up to 30 in various PELs, and all the results collapse to the universal line of Eq. (4).

The universality revealed by experiments is limited by two factors. The first factor is the variety of PELs that can be realized by optical tweezers or solid background particles. These PELs are largely combinations of pointlike potentials. To some extent, defocused lasers can blur point traps to form more smooth PELs, but at the cost of a smaller range for diffusion dynamics [diamonds in Fig. 3(a)]. The second factor is the quality of statistics in experiments. Both ϕ and S_N depend on the accurate measurement of the probability density of particles at each location. For PELs with large fluctuations and slow dynamics, the frequency of diffusing particles visiting high potential energy regions is exponentially low, which leads to insufficient statistics in these regions and errors in the estimations of both P_i and $U(r)$. These limitations in experiments are remedied by molecular dynamics simulations, where a wider range of PELs are tested with substantially improved statistics.

Figure 4(a) shows the normalized diffusion coefficient as a function of $\phi^{0.5}[(1/S_N) - 1]$ for continuous PELs in simulations. Similar to experiments, all the results collapse to a master curve that can be well fitted to Eq. (4). In Fig. 4(b), simulation results from backgrounds consisting of fixed particles are superimposed on those from continuous PELs with nearly perfect overlap. Compared with experiments, simulations show a much tighter collapse of the data as the potential energies are analytically prescribed with much higher sampling counts. The dynamic range of the diffusion coefficient is ~54, significantly larger than that in the experiments.

Colloidal experiments and computer simulations have shown that the diffusion dynamics of a particle can be

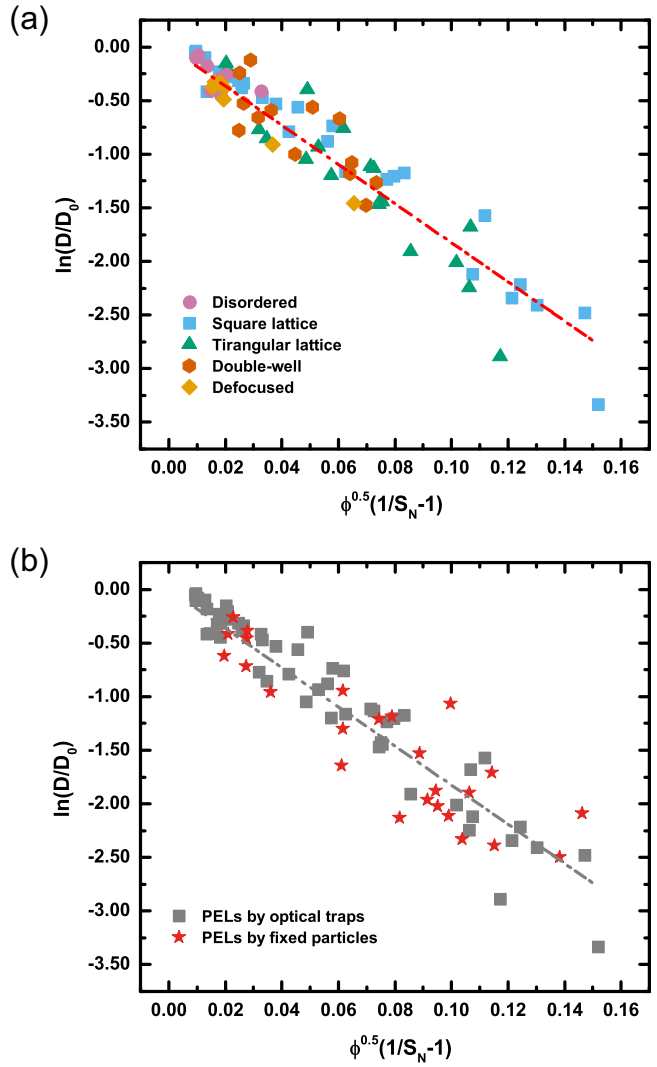

FIG. 3. The normalized long-time diffusion coefficient as a function of $\boldsymbol{\phi}^{0.5}[(1/S_N)-1]$ in experiments. (a) Experimental results from different arrays of optical traps, including disordered arrays of Gaussian traps (pink circles), square lattices (light blue squares), triangular lattices (green triangles), arrays of double wells (orange hexagons), and disordered defocused traps (yellow diamonds). The red dash-dotted line is the linear fit of all the experimental data by Eq. (4). (b) A comparison between the results from backgrounds formed by optical traps (gray squares) and by fixed colloidal particles (red stars). The gray dash-dotted line is the same as the red dash-dotted line in (a).

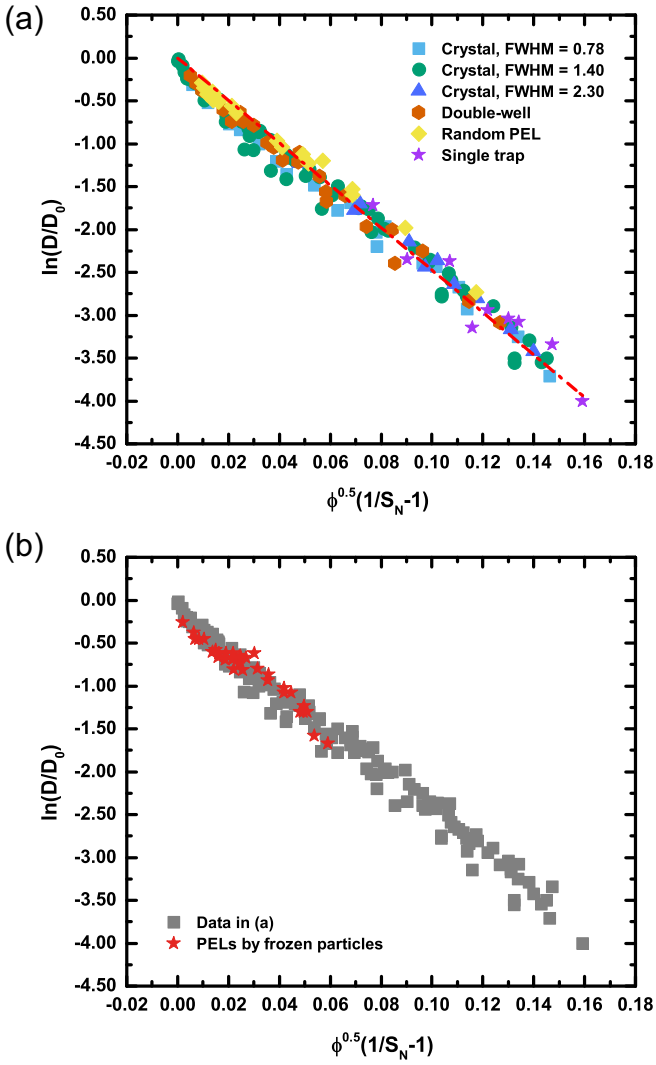

FIG. 4. The normalized long-time diffusion coefficient as a function of $\boldsymbol{\phi}^{0.5}[(1/S_N)-1]$ in simulations. (a) Simulation results from arrays of attractive traps and continuous PELs, including crystalline lattices of Gaussian traps of different shapes characterized by the full width at half maximum (FWHM) of the potential function (light blue squares, green circles, dark blue triangles), arrays of double-well traps (orange hexagons), and single Gaussian traps with large FWHMs (purple stars). The red dash-dotted line is the linear fit of all the simulation data by Eq. (4). (b) A comparison between the data in (a) (gray solid squares) and particles diffusing in PELs of frozen particles (red stars).

uniquely determined by the shape of the PEL using Eq. (4). The obtained universal slope α_0 is 18.26 for experiments and 24.74 for simulations. The steeper slope in simulations implies higher sensitivity of the dynamics to the change of PELs, due to the substantially higher statistics and analytically accurate PELs. Both ϕ and S_N characterize the spatial fluctuations in the PEL. Large fluctuations lead to higher ϕ and lower S_N, thus slower dynamics. Similar to the packing fraction in hard-sphere packings, ϕ is a geometrical parameter that measures the size of the local features in the PEL that significantly hinder the free diffusion of particles. In continuous PELs, both an energy barrier (e.g., a solid particle) and a potential well (e.g., an optical trap) slow down the diffusion of a particle, and are accounted for symmetrically in ϕ. The information entropy S_N, on the other hand, is a statistical parameter that quantifies the order in the structure of the PEL. The contributions to S_N from positive barriers and negative wells are not symmetric, as a negative well introduces more order than a positive

barrier. This comparison is most clear in the extreme cases of an infinitely deep well and a hard-sphere obstacle in a finite space, with long-time diffusion coefficient $D \to 0$ in the former and $D \approx D_0$ in the latter.

Thus, Eq. (4) clarifies a common misunderstanding about the crowding effects in the slowing down of dynamics in colloidal systems with packing fractions. Even though larger ϕ leads to slower dynamics, the value of ϕ is bounded by unity so that D/D_0 cannot become arbitrarily small by increasing ϕ alone. The drastic slowing down of diffusing dynamics observed during colloidal glass transition is therefore not the direct results of increased ϕ, as it has often been attributed to, but from the sharp fluctuations in energy landscape that substantially decreases the system entropy when particles come into contact with each other. At this point, ϕ is no longer an effective proxy for the PEL, while S_N becomes the dominant factor in determining the dynamics. Similar analysis can be applied to molecular glass transitions. In practice, glass transitions are usually determined by an endothermic peak during differential scanning calorimetry measurements which indicates a sudden increase in system entropy accompanied by a sharp increase of system dynamics, while common structural measures such as density ρ or structural factor $S(q)$ exhibit little change.

In this Letter, we study the simple case of a particle diffusing in static unbiased PELs at 2D. The diffusion coefficients of colloidal particles in PELs constructed by optical tweezers or fixed particles can be uniquely determined by a universal law that employs Shannon information entropy and generalized packing fraction derived from the PELs. This universal law is tested and validated in more complex PELs by computer simulations. As entropy is a measure of order in statistical systems, this general law reveals the deep connection between the thermodynamics and dynamics in complex systems, which is relevant to many problems in condensed matter physics such as the glass transition. Despite the remarkable universality demonstrated in experiments and simulations, Eq. (4) remains empirical and requires further theoretical and experimental investigations. Theoretically, it would be useful to derive this relation analytically and clarify the meanings of α_0, ϕ, and S_N, or to identify additional parameters relevant to diffusing dynamics. To extend Eq. (4) to wider scenarios in experiments, several issues need to be addressed, including the effects of time-dependent PELs, biased PELs with internal or external drivings, and the equivalence between information entropy and thermodynamic entropy.

Acknowledgments—We thank David Dean for helpful discussions. This work is supported by the National Natural Science Foundation of China (Grants No. 12174434 and No. 12304245).

Data availability—The data that support the findings of this article are not publicly available upon publication because it is not technically feasible and/or the cost of preparing, depositing, and hosting the data would be prohibitive within the terms of this research project. The data are available from the authors upon reasonable request.

[1] Y. Li, J. Qian, M. Zhang, S. Wang, Z. Wang, M. Li, Y. Bai, Q. An, H. Xu, F. Wu *et al.*, Adv. Mater. **32**, 2005802 (2020).
[2] Y. Shen, Y. Jiang, Z. Yang, J. Dong, W. Yang, Q. An, and L. Mai, Adv. Sci. **9**, 2104504 (2022).
[3] F. Yang, L. Xu, Y. Gao, C. Chen, C. Lu, and F. Wang, J. Colloid Interface Sci. **641**, 176 (2023).
[4] J. Vrentas and J. Duda, Macromolecules **9**, 785 (1976).
[5] O. Karlsson, J. Stubbs, L. Karlsson, and D. Sundberg, Polymer **42**, 4915 (2001).
[6] A. S. Verkman, Trends Biochem. Sci. **27**, 27 (2002).
[7] J. T. Mika and B. Poolman, Curr. Opin. Biotechnol. **22**, 117 (2011).
[8] I. S. Santos de Oliveira, W. K. den Otter, and W. J. Briels, J. Chem. Phys. **137**, 204908 (2012).
[9] A. Nicolas and M. Fuchs, J. Non-Newtonian Fluid Mech. **228**, 64 (2016).
[10] J. R. Gomez-Solano, A. Blokhuis, and C. Bechinger, Phys. Rev. Lett. **116**, 138301 (2016).
[11] L. M. McDowell-Boyer, J. R. Hunt, and N. Sitar, Water Resour. Res. **22**, 1901 (1986).
[12] C. K. Ho and S. W. Webb, *Gas Transport in Porous Media* (Springer, Dordrecht, 2006), Vol. 20.
[13] L. Chen, A. He, J. Zhao, Q. Kang, Z.-Y. Li, J. Carmeliet, N. Shikazono, and W.-Q. Tao, Prog. Energy Combust. Sci. **88**, 100968 (2022).
[14] G. Tarjus and D. Kivelson, J. Chem. Phys. **103**, 3071 (1995).
[15] L. Berthier, Physics **4** (2011).
[16] F. Godey, A. Fleury, and A. Soldera, Sci. Rep. **9**, 9638 (2019).
[17] H. Scher and M. Lax, Phys. Rev. B **7**, 4491 (1973).
[18] J. Bernasconi, H. U. Beyeler, S. Strässler, and S. Alexander, Phys. Rev. Lett. **42**, 819 (1979).
[19] J. W. Haus, K. W. Kehr, and J. W. Lyklema, Phys. Rev. B **25**, 2905 (1982).
[20] M. Schmiedeberg, J. Roth, and H. Stark, Eur. Phys. J. E **24**, 367 (2007).
[21] D. S. Dean, I. T. Drummond, and R. R. Horgan, J. Stat. Mech. (2007) P07013.
[22] S. Lifson and J. L. Jackson, J. Chem. Phys. **36**, 2410 (1962).
[23] R. Zwanzig, Proc. Natl. Acad. Sci. U.S.A. **85**, 2029 (1988).
[24] W. Dieterich, I. Peschel, and W. Schneider, Z. Phys. B **27**, 177 (1977).
[25] K. Seki and B. Bagchi, J. Chem. Phys. **143**, 194110 (2015).
[26] Y. Rosenfeld, Phys. Rev. A **15**, 2545 (1977).
[27] Y. Rosenfeld, J. Phys. Condens. Matter **11**, 5415 (1999).
[28] M. Dzugutov, Nature (London) **381**, 137 (1996).
[29] S. M. Ali, A. Samanta, and S. K. Ghosh, J. Chem. Phys. **114**, 10419 (2001).
[30] A. Samanta, Sk. Musharaf Ali, and S. K. Ghosh, Phys. Rev. Lett. **87**, 245901 (2001).
[31] A. Samanta, Sk. Musharaf Ali, and S. K. Ghosh, Phys. Rev. Lett. **92**, 145901 (2004).

[32] L. Ning, P. Liu, Y. Zong, R. Liu, M. Yang, and K. Chen, Phys. Rev. Lett. **122**, 178002 (2019).
[33] B. Sorkin, H. Diamant, and G. Ariel, Phys. Rev. Lett. **131**, 147101 (2023).
[34] See Supplemental Material at http://link.aps.org/supplemental/10.1103/39zl-5pn3 for additional details on creation of complex PELs in simulations, evaluation of D, S_N, and ϕ, comparison with existing theoretical models, bin number dependence, and entropy for negative delta potentials, which includes Refs. [21,35,36]
[35] I. R. Cooke, K. Kremer, and M. Deserno, Phys. Rev. E **72**, 011506 (2005).
[36] R. H. Kraichnan, J. Fluid Mech. **77**, 753 (1976).
[37] G. Adam and J. H. Gibbs, J. Chem. Phys. **43**, 139 (1965).